Preprints of the 19th World Congress
The International Federation of Automatic Control
Cape Town, South Africa. August 24-29, 2014

Quasi optimal feedforward control of a very low frequency high-voltage test system ⋆

W. Kemmetmüller * **S. Eberharter** * **A. Kugi** *

* *Automation and Control Institute, Vienna University of Technology, Gußhausstrasse 27-29, 1040 Vienna, Austria (e-mail: {eberharter, kemmetmueller, kugi}@acin.tuwien.ac.at).*

Abstract: This paper presents the design of a quasi optimal feedforward controller for a new type of high-voltage test systems. Compared to existing solutions, this test system has the advantage of a compact lightweight construction and is thus particularly suitable for on-site tests. For system analysis and controller design, a tailored mathematical model is derived, which describes the (slow) envelope dynamics of the occurring amplitude modulated signals. The proposed (quasi optimal) control concept ensures a simultaneous minimization of the mean power losses and of the distortion of the output voltage. Simulation results for a validated mathematical model show the feasibility of the approach.

Keywords: high-voltage test systems, envelope model, optimal control, feedforward control.

1. INTRODUCTION

In recent years, a forced expansion of regenerative energy production by means of large scale wind parks, photovoltaic or biomass power plants is reported. These mostly decentralized systems are often connected to the electricity distribution network by high- and ultra-high-voltage cables. In order to guarantee a fail-safe energy supply, the cables have to pass strict quality tests, such as factory acceptance tests and on-site tests of already installed cables. For the on-site cable tests, the test devices have to provide a compact and lightweight construction. Because of this, a new type of cable test method with very low frequencies (VLF) in the range of 0.01 Hz to 0.1 Hz was recently established, which reduces the amount of reactive power and, therefore, the size and weight of the test devices, see Putter et al. (2012); IEEE Power Engineering Society (2004); Pietsch and Hausschild (2005); Krüger et al. (1990); Muhr et al. (2001); Coors and Schierig (2008). The company Mohaupt High Voltage GmbH developed a new type of VLF test system based on the so called Differential Resonance Technology (DRT), which allows a mobile VLF testing of cables up to 500 kV rms and higher, see Mohaupt et al. (2012); Mohaupt and Bergmann (2010). The functional principle of this new test system is depicted in Figure 1. Therein, the resonant circuit is tuned to its resonance by the two pulse width modulated input voltages u_{p1} and u_{p2} generated by the power module. The choice of the two input frequencies, $\omega_{p1} = \omega_r - \omega_\Delta$ and $\omega_{p2} = \omega_r + \omega_\Delta$, results in an amplitude modulated (AM) high-voltage u_r across the resonant capacitor. This high-voltage signal comprises a carrier frequency ω_r and the desired low frequency ω_Δ of the test signal u_l. By a defined switching of the thyristors in the demodulator (SVU - switched valve unit), the desired high voltage test signal u_l with the low frequency ω_Δ is generated. In order

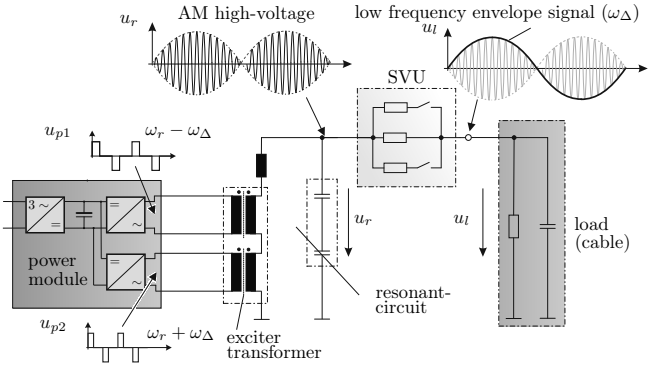

Fig. 1. Functional principle of the DRT test system.

to fulfill the high quality standards of cable test voltages, e.g. the distortion factor (see IEC 60060-1 and IEC 60060-3), and to allow an energy efficient operation, a suitable control of the DRT system is needed.

This paper deals with the development of a feedforward control for the amplitude and shape of the test voltage of the DRT system. The control strategy is based on an envelope model of the DRT test system, which is derived in Section 2. In Section 3, the model will be used to analyze the behavior and dynamics of the DRT system, especially the behavior during the demodulation of u_l. Based on this formulation, an optimal control problem is solved by minimizing the mean power losses of the DRT system. The results of the optimal control problem serve as a basis for the design of a realtime-capable quasi optimal feedforward control, which is validated by simulations. Conclusions are drawn in Section 4.

⋆ The research for this paper has been sponsored by the FFG-Austrian Research Promotion Agency in the BRIDGE-project no. 829582. Further thanks go to Peter Mohaupt and the employees of Mohaupt High Voltage GmbH for supporting the measurement campaigns.

2. MATHEMATICAL MODELING

The following section is concerned with the mathematical modeling of the DRT test system. In a first step a simplified model, considering the essential physical behavior of the system, will be derived. Based on this model an envelope model is developed. For more detailed information on the modeling and the analysis of the DRT system, see Eberharter et al. (2013).

2.1 Simplified model

An equivalent circuit diagram of the DRT system described in Section 1 is shown in Figure 2. The model is

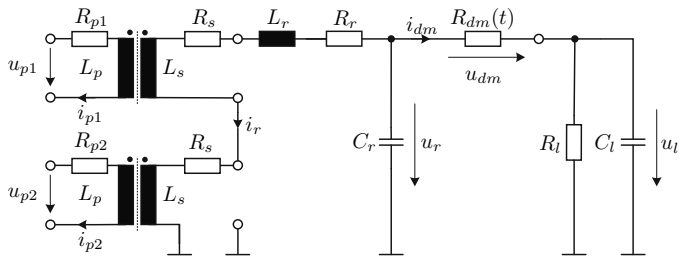

Fig. 2. Circuit diagram of the DRT system with a continuously adjustable demodulator resistor $R_{dm}(t)$.

based on the following assumptions and simplifications: (i) The overall demodulator is described by a continuously variable resistor $R_{dm}(t)$. By means of a defined switching sequence of the thyristors, the value of $R_{dm}(t)$ can be varied between R_{on} and R_{off}. (ii) The exciter is supplied by the tunable voltages of the power module u_{p1} and u_{p2}.

The primary currents i_{p1} and i_{p2} of the exciter transformers and the resonator current i_r are given by the following differential equations

$$\mathbf{L}\frac{\mathrm{d}}{\mathrm{d}t}\begin{bmatrix} i_{p1} \\ i_{p2} \\ i_r \end{bmatrix} = \begin{bmatrix} -R_p i_{p1} + u_{p1} \\ -R_p i_{p2} + u_{p2} \\ -\left(2R_s + R_r\right) i_r + u_r \end{bmatrix}, \tag{1}$$

with the primary and secondary resistance R_p and R_s of the exciter transformers, the resistance of the resonant circuit R_r, the resonant voltage u_r and the inductance matrix $\mathbf{L}$, which is given by

$$\mathbf{L} = \begin{bmatrix} L_p & 0 & L_{ps} \\ 0 & L_p & L_{ps} \\ L_{ps} & L_{ps} & 2L_s + L_r \end{bmatrix}. \tag{2}$$

Therein, L_p and L_s describe the primary and secondary inductance of the exciter transformer, L_r is the resonant inductance and $L_{ps} = k\sqrt{L_p L_s}$ is the coupling inductance with the coupling factor $k < 1$. The resonator voltage u_r is described by

$$\frac{\mathrm{d}u_r}{\mathrm{d}t} = \frac{1}{C_r}\left(-i_r - i_{dm}\right), \tag{3}$$

with the current i_{dm} through the demodulator. Given a high-voltage cable with a constant capacitance C_l and an ohmic resistance R_l, the output voltage u_l can be written as

$$\frac{\mathrm{d}u_l}{\mathrm{d}t} = \frac{1}{C_l}\left(-\frac{u_l}{R_l} + i_{dm}\right). \tag{4}$$

As mentioned before, a simplified model of the demodulator is summarized in this section, for more details see Eberharter et al. (2013). The behavior of the thyristors is described by switchable ideal diodes with a negligible on-resistance and vanishing threshold voltage. Thus, the positive and negative branches of the demodulator are given by adjustable resistors R_{dm}^{+} and R_{dm}^{-} and the current i_{dm} through the demodulator reads as

$$i_{dm} = \begin{cases} \dfrac{u_{dm}}{R_{dm}^{+}} & \text{if } u_{dm} \geq 0 \\ \dfrac{u_{dm}}{R_{dm}^{-}} & \text{if } u_{dm} < 0, \end{cases} \tag{5}$$

with the demodulator voltage $u_{dm} = u_r - u_l$ and $R_{dm}^{+}, R_{dm}^{-} \in [R_{on}, R_{off}]$. Equation (5) can be rewritten as

$$i_{dm} = \frac{1}{R_{off}}u_{dm} + \left(\frac{1}{R_{dm}^{+}} - \frac{1}{R_{off}}\right)g^{+} + \left(\frac{1}{R_{dm}^{-}} - \frac{1}{R_{off}}\right)g^{-}, \tag{6}$$

with g^{+} and g^{-} defined as

$$g^{+} = \begin{cases} u_{dm} & \text{if } u_{dm} \geq 0 \\ 0 & \text{if } u_{dm} < 0 \end{cases}, \qquad g^{-} = u_{dm} - g^{+}. \tag{7}$$

The primary voltages u_{p1} and u_{p2} of the exciter coils are generated by two full-bridges in the power module. They have a pulse-width modulated rectangular shape with a fixed amplitude u_p and adjustable duty cycles χ_1 and χ_2, which can be varied in the range of $0 \leq \chi_1, \chi_2 \leq 1$. The desired amplitude modulation of the resonant voltage u_r is achieved by the choice of the cycle times T_{p1} and T_{p2} of the power module voltages according to

$$T_{p1} = \frac{2\pi}{\omega_{p1}} = \frac{2\pi}{\omega_r - \omega_\Delta}, \qquad T_{p2} = \frac{2\pi}{\omega_{p2}} = \frac{2\pi}{\omega_r + \omega_\Delta}. \tag{8}$$

2.2 Envelope model

For the system analysis and the development of a control strategy, it is reasonable to use an envelope model, which only describes the time evolution of the envelopes, i.e. the time profile of the mean value and the amplitude of the high frequency signal produced by the serial resonant circuit, see, e.g., Caliskan et al. (1996); Sanders and Verhulst (1985); Egretzberger and Kugi (2010).

Therefore, the system state variables of the mathematical model are approximated by a slowly time varying mean component $X_0(t)$, a cosine $X_c(t)$ and a sine component $X_s(t)$ in the form

$$x(t) = X_0(t) + X_c(t)\cos(\omega_r t) + X_s(t)\sin(\omega_r t), \tag{9}$$

where ω_r is the high frequency of the carrier signal. With this definition, the system state $x(t)$ can be written as

$$x(t) = \mathbf{X}(t)\mathbf{w}(t), \tag{10}$$

with

$$\mathbf{X}(t) = \left[X_0(t)\ X_C(t)\ X_S(t)\right], \qquad \mathbf{w}(t) = \begin{bmatrix} 1 \\ \cos(\omega_r t) \\ \sin(\omega_r t) \end{bmatrix}. \tag{11}$$

The time derivative of (11) results in

$$\dot{x}(t) = \dot{\mathbf{X}}(t)\mathbf{w}(t) + \mathbf{X}(t)\dot{\mathbf{w}}(t), \tag{12}$$

where $\dot{\mathbf{w}}(t)$ can be expressed as

$$\dot{\mathbf{w}} = \begin{bmatrix} 0 \\ -\omega_r \sin(\omega_r t) \\ \omega_r \cos(\omega_r t) \end{bmatrix} = \begin{bmatrix} 0 & 0 & 0 \\ 0 & 0 & -\omega_r \\ 0 & \omega_r & 0 \end{bmatrix} \begin{bmatrix} 1 \\ \cos(\omega_r t) \\ \sin(\omega_r t) \end{bmatrix} = \mathbf{\Omega}\mathbf{w}. \tag{13}$$

As will be shown, a regular state transformation $i_\Sigma = i_{p1} + i_{p2}$, $i_\Delta = i_{p1} - i_{p2}$ and $i_r = i_r$ with the new system inputs $u_\Sigma = u_{p1} + u_{p2}$ and $u_\Delta = u_{p1} - u_{p2}$ is useful in view of a system analysis. Applying this state transformation to the mathematical model of Section 2.1 and using (10)-(13), the envelope model of the currents i_Σ, i_r, i_Δ results in

$$\mathbf{L}_{\Sigma r}\frac{\mathrm{d}}{\mathrm{d}t}\begin{bmatrix}\mathbf{I}_r\\ \mathbf{I}_\Sigma\end{bmatrix} = -\mathbf{L}_{\Sigma r}\begin{bmatrix}\mathbf{I}_r\\ \mathbf{I}_\Sigma\end{bmatrix}\mathbf{\Omega} - \begin{bmatrix}2R_s+R_r & 0\\ 0 & R_p\end{bmatrix}\begin{bmatrix}\mathbf{I}_r\\ \mathbf{I}_\Sigma\end{bmatrix} + \begin{bmatrix}\mathbf{U}_r\\ \mathbf{U}_\Sigma\end{bmatrix} \tag{14a}$$

$$L_p\frac{\mathrm{d}}{\mathrm{d}t}\mathbf{I}_\Delta = -L_p\mathbf{I}_\Delta\mathbf{\Omega} - R_p\mathbf{I}_\Delta + \mathbf{U}_\Delta, \tag{14b}$$

wherein $\mathbf{L}_{\Sigma r}$ is the reduced inductance matrix

$$\mathbf{L}_{\Sigma r} = \begin{bmatrix}2L_s + L_r & L_{ps}\\ 2L_{ps} & L_p\end{bmatrix}. \tag{15}$$

The vectors $\mathbf{U}_\Sigma, \mathbf{U}_\Delta, \mathbf{U}_r, \mathbf{I}_\Sigma, \mathbf{I}_\Delta$ and $\mathbf{I}_r$ combine the corresponding envelope coefficients as defined in (11).

The envelope model of the voltages u_r and u_l can be written according to (3) and (4) in the form

$$\frac{\mathrm{d}}{\mathrm{d}t}\mathbf{U}_r = -\mathbf{U}_r\mathbf{\Omega} + \frac{1}{C_r}\left(-\mathbf{I}_r - \mathbf{I}_{dm}\right) \tag{16a}$$

$$\frac{\mathrm{d}}{\mathrm{d}t}\mathbf{U}_l = -\mathbf{U}_l\mathbf{\Omega} + \frac{1}{C_l}\left(-\frac{1}{R_l}\mathbf{U}_l + \mathbf{I}_{dm}\right). \tag{16b}$$

The envelope coefficients of the new system inputs $\mathbf{U}_\Sigma$ and $\mathbf{U}_\Delta$ with $\chi_1 = \chi_2 = \chi$ are calculated by

$$U_{\Sigma,0} = 0 \tag{17a}$$

$$U_{\Sigma,c} = \frac{4}{\pi}\sin(\chi\pi)\cos(\omega_\Delta t)\,u_p \tag{17b}$$

$$U_{\Sigma,s} = \frac{4}{\pi}\left(1-\cos(\chi\pi)\right)\cos(\omega_\Delta t)\,u_p \tag{17c}$$

and

$$U_{\Delta,0} = 0 \tag{18a}$$

$$U_{\Delta,c} = \frac{4}{\pi}\left(-1+\cos(\chi\pi)\right)\sin(\omega_\Delta t)\,u_p \tag{18b}$$

$$U_{\Delta,s} = \frac{4}{\pi}\sin(\chi\pi)\sin(\omega_\Delta t)\,u_p. \tag{18c}$$

To complete the description of the envelope model, the current through the demodulator $\mathbf{I}_{dm}$, which is a function of the demodulator voltage $\mathbf{U}_{dm}$ and the demodulator resistors R^+_{dm} and R^-_{dm}, needs to be calculated. Given (6), the current $\mathbf{I}_{dm}$ of the envelope model can be written as

$$\mathbf{I}_{dm} = \frac{1}{R_{off}}\mathbf{U}_{dm} + \left(\frac{1}{R^+_{dm}} - \frac{1}{R_{off}}\right)\mathbf{G}^+ + \left(\frac{1}{R^-_{dm}} - \frac{1}{R_{off}}\right)\mathbf{G}^-, \tag{19}$$

with $\mathbf{G}^- = \left[G^-_0,\, G^-_c,\, G^-_s\right]$, $\mathbf{G}^+ = \left[G^+_0,\, G^+_c,\, G^+_s\right]$ and $\mathbf{U}_{dm} = \mathbf{U}_r - \mathbf{U}_l$. The envelope coefficients of g^+ and g^- are calculated by means of the periodic Fourier transformation (Papoulis (1962)) applied to (7). In order to evaluate the resulting integrals, the conditions $u_{dm} \geq 0$ and $u_{dm} < 0$ must be described in terms of the envelope coefficients $U_{dm,0}, U_{dm,c}$ and $U_{dm,s}$. Here, it is assumed that $U_{dm,0}(t)$, $U_{dm,c}(t)$ and $U_{dm,s}(t)$ are constant for the integration interval $0, \ldots, \frac{2\pi}{\omega_r}$. The nonlinear terms of $\mathbf{G}^+$ result in

$$G^+_0 = \left(1 - \frac{\arccos\left(\frac{U_{dm,0}}{\hat{U}_{dm}}\right)}{\pi}\right)U_{dm,0} + \frac{\sqrt{\hat{U}^2_{dm} - U^2_{dm,0}}}{\pi} \tag{20a}$$

$$G^+_c = \left(1 - \frac{\arccos\left(\frac{U_{dm,0}}{\hat{U}_{dm}}\right)}{\pi}\right)U_{dm,c} + \frac{\sqrt{\hat{U}^2_{dm} - U^2_{dm,0}}}{\pi}\frac{U_{dm,0}U_{dm,c}}{\hat{U}^2_{dm}} \tag{20b}$$

$$G^+_s = \left(1 - \frac{\arccos\left(\frac{U_{dm,0}}{\hat{U}_{dm}}\right)}{\pi}\right)U_{dm,s} + \frac{\sqrt{\hat{U}^2_{dm} - U^2_{dm,0}}}{\pi}\frac{U_{dm,0}U_{dm,s}}{\hat{U}^2_{dm}}, \tag{20c}$$

with $\hat{U}_{dm} = \sqrt{U^2_{dm,c} + U^2_{dm,s}}$. The nonlinear terms of $\mathbf{G}^-$ can be calculated by $\mathbf{G}^- = \mathbf{U}_{dm} - \mathbf{G}^+$. These results are valid in the interval $-\hat{U}_{dm} \leq U_{dm,0} \leq \hat{U}_{dm}$. In the case $U_{dm,0} > \hat{U}_{dm}$, the envelope coefficients of $\mathbf{G}^+$ and $\mathbf{G}^-$ are given by

$$G^+_0 = U_{dm,0}, \quad G^+_c = U_{dm,c}, \quad G^+_s = U_{dm,s} \tag{21a}$$

$$G^-_0 = 0, \quad G^-_c = 0, \quad G^-_s = 0 \tag{21b}$$

and for $U_{dm,0} < -\hat{U}_{dm}$ they read as

$$G^+_0 = 0, \quad G^+_c = 0, \quad G^+_s = 0 \tag{22a}$$

$$G^-_0 = U_{dm,0}, \quad G^-_c = U_{dm,c}, \quad G^-_s = U_{dm,s}. \tag{22b}$$

The envelope model is validated by a comparison with the

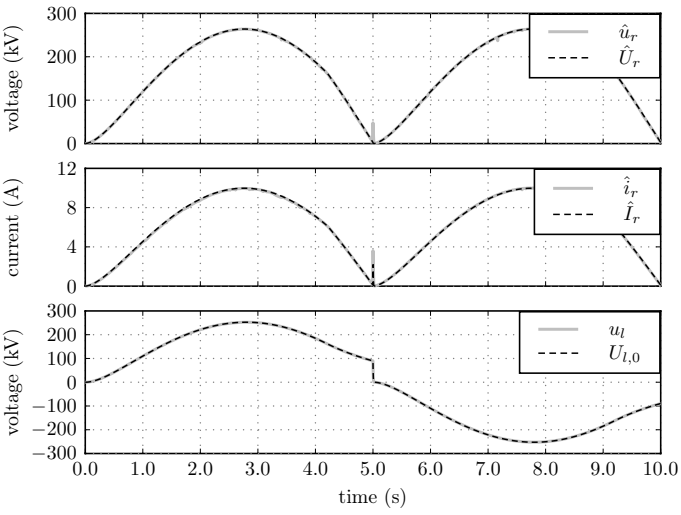

Fig. 3. Comparison of the envelope model with the simplified model of Section 2.1.

model of Section 2.1, which has already been calibrated by measurements, cf. Eberharter et al. (2013). Both models were simulated with a resistive-capacitive load of $R_l = 300\,\mathrm{M\Omega}$, $C_l = 150\,\mathrm{nF}$ and the power module pulse widths $\chi = 0.28$. For the generation of the output voltage u_l, a simple demodulation strategy was used, where all thyristors of the positive branch are switched on for the positive half-wave of u_l and all thyristors of the negative branch are switched on for the negative half-wave. To allow a better comparison of both models, the results

of the envelope model are compared with the envelopes of the signals of the simplified model in Figure 3. Due to the nonlinearities of the demodulator, a distortion of the sinusoidal shapes of the currents and voltages in the resonant circuit occurs. Nevertheless, as can be seen in Figure 3, this deviation is negligible such that the envelope model is a very good approximation of the simplified model.

3. CONTROL STRATEGY

To develop a suitable control strategy, the behavior of the DRT system is analyzed by means of the envelope model of Section 2.2. Subsequently, an optimization problem is formulated which is the basis for the development of a quasi optimal feedforward control. In this paper, it is presumed that the voltage u_r ideally tracks a desired voltage u_r^d. Thus, u_r can be used as a virtual control input and the series resonant circuit and the power module can be neglected. Consequently, the output voltage u_l has to be controlled by changing the new (virtual) control inputs u_r, R_{dm}^+ and R_{dm}^-.

3.1 System analysis

For the system analysis the simple demodulation strategy of the last section is considered again. Furthermore, the analysis is only carried out for the positive half-wave of u_l, since the negative half-wave can be treated in similar manner. The following questions will be discussed in detail:

(I) How to choose the resonant voltage u_r and accordingly the amplitude $\hat{U}_r$ to minimize the error between the output voltage u_l and a desired sinusoidal trajectory u_l^d?
(II) How large is the amplitude $\hat{U}_l$ of the expected output voltage ripple (distortion factor)?

In order to address these questions the following assumptions are made: (i) The average value of u_r is zero, i.e. $U_{r,0} = 0$ and thus $U_{dm,0} = -U_{l,0}$. (ii) The voltage ripple of the output voltage u_l is neglected, i.e. $U_{l,c} = U_{l,s} = 0$ and thus $\hat{U}_{dm} = \hat{U}_r$. (iii) The desired output voltage is sinusoidal $u_l^d(t) = U_{l,0}^d = \hat{U}_{l,0}^d \sin(\omega_\Delta t)$.

Using these assumptions and $R_{dm}^+ = R_{on}$, $R_{dm}^- = R_{off}$ in (16b) for $U_{l,0}$ and (19) for $I_{dm,0}$, (16b) can be solved with $G_0^- = U_{dm,0} - G_0^+$ for G_0^+,

$$G_0^+\left(\hat{U}_{dm}, U_{dm,0}\right) \approx G_0^+\left(\hat{U}_r, -U_{l,0}\right) = \frac{C_l \dot{U}_{l,0} + \left(\frac{1}{R_l} + \frac{1}{R_{dm}^-}\right) U_{l,0}}{\left(\frac{1}{R_{dm}^+} - \frac{1}{R_{dm}^-}\right)}. \tag{23}$$

With the description of G_0^+ from (20a), (23) can be solved numerically for $\hat{U}_r$ as long as the right hand side of (23) is greater than zero.

Figure 4 depicts a desired sinusoidal output voltage $u_l^d(t) = U_{l,0}^d$ and the required amplitude $\hat{U}_r$ for a load of $C_l = 500\,\mathrm{nF}$ and $R_l = 300\,\mathrm{M\Omega}$. As can be seen, the amplitude $\hat{U}_r$ has to be slightly larger than the amplitude $\hat{U}_{l,0}^d$ of the desired output voltage in order to compensate for the ohmic losses in the demodulator. Furthermore, Figure 4 shows that no solution for $\hat{U}_r$ can be found for $t > 3\,\mathrm{s}$. This means that a control of the output voltage by simply adjusting the voltage u_r does not work for the whole period of the sinusoidal output voltage. Thus, an active change of R_{dm}^+ and R_{dm}^- is necessary for $t > 3\,\mathrm{s}$.

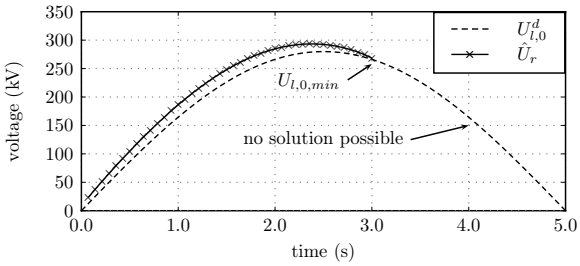

Fig. 4. Required amplitude $\hat{U}_r$ for a desired sinusoidal output voltage $U_{l,0}^d$.

The second part of the analysis is concerned with the output voltage ripple $\hat{U}_l$. For this purpose, a transformation to amplitude and phase angle in the form $U_{l,c} = \hat{U}_l \cos(\varphi_l), U_{l,s} = \hat{U}_l \sin(\varphi_l), U_{dm,c} = \hat{U}_{dm} \cos(\varphi_l + \varphi_{dm})$ and $U_{dm,s} = \hat{U}_{dm} \sin(\varphi_l + \varphi_{dm})$ is applied to (16b) and (19). Under the assumptions made at the beginning of this subsection, this results in

$$\frac{\mathrm{d}}{\mathrm{d}t}\hat{U}_l = \frac{1}{C_l}\left[\left(\frac{1}{R_{on}} - \frac{1}{R_{off}}\right)\hat{G}^+ + \frac{1}{R_{off}}\hat{U}_{dm}\right]\cos(\varphi_{dm}) - \frac{1}{R_l C_l}\hat{U}_l \tag{24a}$$

$$\frac{\mathrm{d}}{\mathrm{d}t}\varphi_l = \frac{1}{\hat{U}_l C_l}\left[\left(\frac{1}{R_{on}} - \frac{1}{R_{off}}\right)\hat{G}^+ + \frac{1}{R_{off}}\hat{U}_{dm}\right]\sin(\varphi_{dm}) + \omega_r, \tag{24b}$$

with $\hat{G}^+ = \sqrt{(G_c^+)^2 + (G_s^+)^2}$. In order to get a first approximation of the output voltage ripple $\hat{U}_l$, a quasi-stationary solution of (24) is sufficient. This is justified by the fact that the dynamics of the voltage ripple is much faster than the dynamics of $U_{l,0}$. This approximation leads to

$$\hat{U}_l = \frac{\frac{1}{C_l}\left[\left(\frac{1}{R_{on}} - \frac{1}{R_{off}}\right)\hat{G}^+ + \frac{1}{R_{off}}\hat{U}_{dm}\right]}{\sqrt{\omega_r^2 + \left(\frac{1}{R_l C_l}\right)^2}}. \tag{25}$$

Remark 1. Since in general $\hat{U}_{dm}$ depends on $\hat{U}_l$, (25) constitutes an implicit nonlinear equation for $\hat{U}_l$. However, in view of assumption (ii) at the beginning of this subsection, $\hat{U}_{dm}$ can be fairly well approximated by $\hat{U}_r$.

Figure 5 depicts the voltage ripple $\hat{U}_l$ for a load of $C_l = 500\,\mathrm{nF}$, $R_l = 300\,\mathrm{M\Omega}$ and the voltages $U_{l,0}^d$ and $\hat{U}_r$ shown in Figure 4. It can be seen that the maximum voltage ripple is less than $2.5\,‰$ of the amplitude of the desired output voltage $U_{l,0}^d$. This is a good result in view of the required high quality standards of cable test voltages. However, it is important to note that Figure 5 only depicts a first approximation of the expected voltage ripple and that the amplitude of this ripple may vary due to other effects, e.g., parasitic effects caused by stray capacities in the housing of the DRT system.

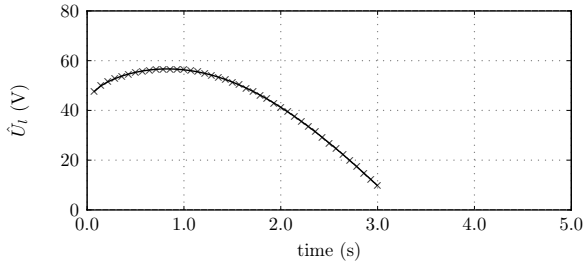

Fig. 5. Output voltage ripple $\hat{U}_l$ for $U_{l,0}^d$ and $\hat{U}_r$ given in Figure 4.

3.2 Optimal control

In the previous system analysis it was shown that a control of u_l only by means of u_r is not possible. Thus, a defined switching of the thyristors in the demodulator, i.e., changing the values of R_{dm}^+ and R_{dm}^- is necessary. In this section, an optimal control problem is formulated to calculate the optimal control input $\mathbf{u}^* = \left[\hat{U}_r^*, R_{dm}^{+,*}, R_{dm}^{-,*}\right]$ such that $U_{l,0}$ tracks a given trajectory $U_{l,0}^d$, while $\hat{U}_l$ and the mean power losses $\bar{p}_{dm}$ in the demodulator are minimized. Since minimizing $\hat{U}_l$ is equal to minimizing $\bar{p}_{dm}$, the resulting static optimization problem can be formulated as

$$\min_{\mathbf{u}} \bar{p}_{dm}\left(\mathbf{u}\right), \tag{26}$$

with the mean power losses $\bar{p}_{dm}$ given by

$$\bar{p}_{dm} = \frac{\omega_r}{2\pi}\int_0^{\frac{2\pi}{\omega_r}} p_{dm}\mathrm{d}t = \\ -U_{l,0}^d I_{dm,0} + \frac{1}{2}U_{r,c}I_{dm,c} + \frac{1}{2}U_{r,s}I_{dm,s} \tag{27}$$

and the nonlinear constraints written as

$$C_l\dot{U}_{l,0}^d + \frac{1}{R_l}U_{l,0}^d + \frac{1}{R_{dm}^-}U_{l,0}^d - \left(\frac{1}{R_{dm}^+} - \frac{1}{R_{dm}^-}\right)G_0^+\left(\mathbf{u}\right) = 0, \\ \begin{bmatrix} R_{on} - R_{dm}^+ \\ R_{dm}^+ - R_{off} \\ R_{on} - R_{dm}^- \\ R_{dm}^- - R_{off} \end{bmatrix} \leq \mathbf{0}. \tag{28}$$

The static optimization problem (26)-(28) is solved using the MATLAB function fmincon with the Interior-Point algorithm. Figure 6 depicts the numerical results for a resistive-capacitive load of $R_l = 300\,\mathrm{M\Omega}$, $C_l = 500\,\mathrm{nF}$, $U_{l,0} = 200\,\mathrm{kV}$ rms, $R_{on} = 25\,\mathrm{k\Omega}$, $R_{off} = 9.3\,\mathrm{M\Omega}$ and a sampling time $T_s = 0.1\,\mathrm{s}$. In the upper part of Figure 6 it can be seen that $\hat{U}_r^*$ has to be slightly larger than $U_{l,0}^d$ during the loading phase of C_l, which confirms the results of the system analysis in Section 3.1. The discharging phase of the load capacity is characterized by $\hat{U}_r^* = 0$. In the lower part of Figure 6, the optimal values of the demodulator resistors R_{dm}^+ and R_{dm}^- are shown. During the loading phase of C_l, the resistors are assigned to their boundary values $[R_{on}, R_{off}]$. To achieve a sinusoidal output voltage, the corresponding demodulator resistor, i.e. R_{dm}^- in the positive half-wave and R_{dm}^+ in the negative half-wave, has to change its value from R_{off} to R_{on} during the discharging of C_l. The value of the opposite demodulator resistor jumps from R_{on} to R_{off} at the beginning of the discharging phase.

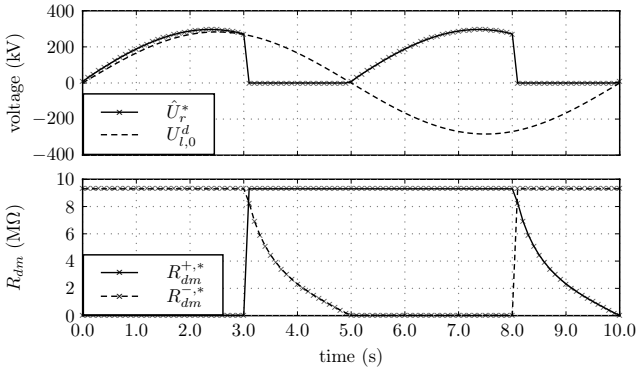

Fig. 6. Numerical results of the optimal control problem for $R_l = 300\,\mathrm{M\Omega}$, $C_l = 500\,\mathrm{nF}$.

The results of this section thus give optimal trajectories for the control inputs. The solution of the optimal control problem, however, is time consuming and not suitable for a realtime implementation. Therefore, a simplified, quasi-optimal control strategy is developed in the next section, which can be easily implemented in realtime.

3.3 Quasi optimal control

The quasi optimal feedforward control relies on the results of the previous section and the assumptions made for the system analysis. For reasons of brevity, the control concept is illustrated for the positive half-wave of u_l only, see Figure 7. It is separated into three phases $\mathbf{A}^+$, $\mathbf{B}^+$ and $\mathbf{C}^+$, where the superscript + refers to he positive half-wave. The three phases can be described as follows:

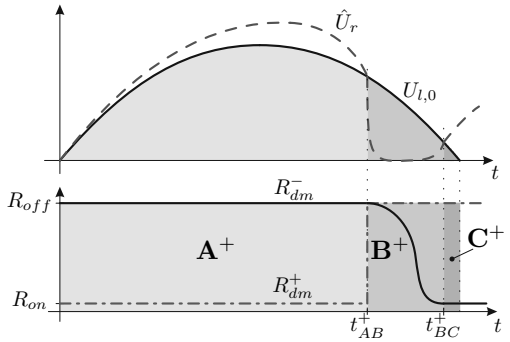

Fig. 7. Phases of the quasi optimal feedforward control.

- **Phase $\mathbf{A}^+$**: C_l is loaded and $U_{l,0}$ is controlled by means of $\hat{U}_r$ with $\hat{U}_r \geq |U_{l,0}|$. The demodulator resistors are chosen as $R_{dm}^+ = R_{on}$ and $R_{dm}^- = R_{off}$. The amplitude $\hat{U}_r$ is calculated using (23), where the numeric solution is simplified by a polynomial approximation of G_0^+ in (20a).
- **Phase $\mathbf{B}^+$**: C_l is discharged and $U_{l,0}$ is controlled by means of the demodulator resistor R_{dm}^- with $\hat{U}_r \leq |U_{l,0}|$. To minimize the power losses in the DRT system, $\hat{U}_r$ is chosen to zero and R_{dm}^+ is set to $R_{dm}^+ = R_{off}$. The value of R_{dm}^- is given by (see (23))

$$R_{dm}^- = -\frac{U_{l,0}^d}{C_l\dot{U}_{l,0}^d + \frac{1}{R_l}U_{l,0}^d}. \tag{29}$$

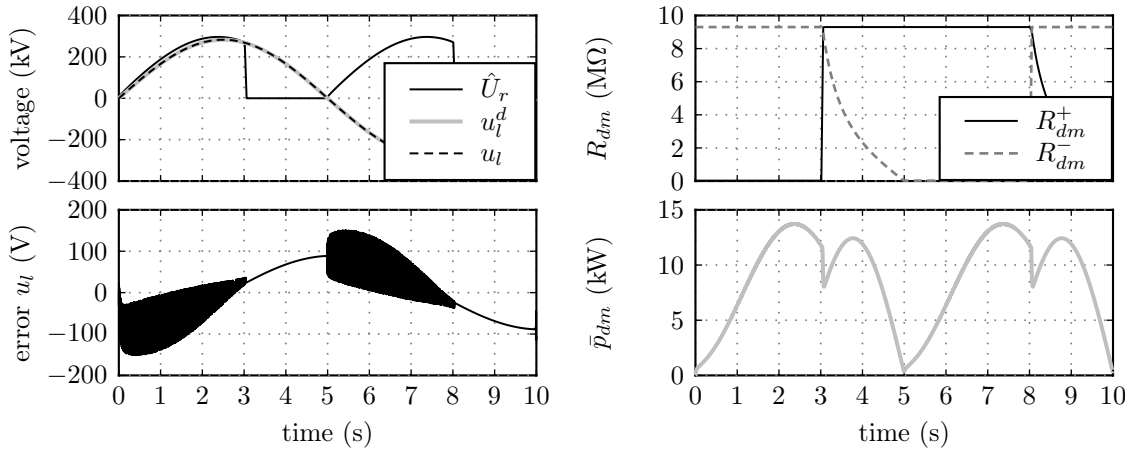

Fig. 8. Simulation results of the quasi optimal feedforward control for $R_l = 300\,\mathrm{M\Omega}$, $C_l = 500\,\mathrm{nF}$.

- **Phase $\mathbf{C}^+$**: C_l is discharged and $U_{l,0}$ is again controlled by means of $\hat{U}_r$, with $\hat{U}_r \geq |U_{l,0}|$. The system input $\hat{U}_r$ is calculated as described in phase $\mathbf{A}^+$, using, however, $R_{dm}^+ = R_{off}$ and $R_{dm}^- = R_{on}$.

The switching times t_{AB}^+ and t_{BC}^+ between the control phases are given by the condition $G_0^+ = 0$. Thus, substituting $U_{l,0} = \hat{U}_{l,0}\sin(\omega_\Delta t)$ into (23) and solving for G_0^+ yields the switching time

$$t_{AB}^+ = \frac{1}{\omega_\Delta}\left(\operatorname{atan}\left(-\frac{\omega_\Delta C_l}{\frac{1}{R_{off}} + \frac{1}{R_l}}\right) + \pi\right), \tag{30}$$

with $R_{dm}^+ = R_{on}$ and $R_{dm}^- = R_{off}$. By analogy, t_{BC}^+ is calculated with $R_{dm}^+ = R_{off}$ and $R_{dm}^- = R_{on}$ to

$$t_{BC}^+ = \frac{1}{\omega_\Delta}\left(\operatorname{atan}\left(-\frac{\omega_\Delta C_l}{\frac{1}{R_{on}} + \frac{1}{R_l}}\right) + \pi\right). \tag{31}$$

For a validation of the quasi optimal feedforward control, the control concept is applied to the mathematical model of Section 2.1 and simulated in MATLAB/SIMULINK. Figure 8 depicts the simulation result for a resistive-capacitive load of $R_l = 300\,\mathrm{M\Omega}$, $C_l = 500\,\mathrm{nF}$, $U_{l,0} = 200\,\mathrm{kV}$ rms and a sampling time $T_s = 3\,\mathrm{ms}$. As can be seen, there is a good agreement between the output voltage u_l and the desired sinusoidal voltage u_l^d with an output error less than 2 ‰ of amplitude of u_l^d. Since the feedforward control was developed based on the envelope model the remaining error can be primarily ascribed to the deviation between the simplified model and the envelope model.

4. CONCLUSIONS AND FUTURE WORK

In this work, a quasi optimal feedforward control of a VLF test system for the testing of high-voltage cables was presented. The feedforward control is based on an optimal control problem, which minimizes the power losses in the test system and the deviation of the test voltage of the ideal sinusoidal shape. In future work, the control concept will be implemented and tested on a prototype designed for cable tests up to 200 kVrms and maximum loads of $C_l = 750\,\mathrm{nF}$. The control concept has to be extended by the control of the resonant voltage u_r by the power module inputs χ_1 and χ_2. Moreover, physical constraints, like the maximum voltage of the thyristors in the SVU, have to be incorporated into the design. Finally, an estimator is under development, which identifies unknown system parameters as, e.g., the capacitance C_l of the test cable.

REFERENCES

Caliskan, V., Verghese, G., and Stankovic, A. (1996). Multifrequency averaging of dc/dc converters. In *Proc. IEEE workshop on computers in power electronics*, 113–119. Portland, USA.

Coors, P. and Schierig, S. (2008). Hv ac testing of super-long cables. In *Proc. of the IEEE Int. Symposium on Electrical Insulation*, 636–640. Vancouver, Canada.

Eberharter, S., Kemmetmüller, W., and Kugi, A. (2013). Mathematical Modeling and Analysis of a Very Low Frequency HV Test System. *IEEE Transactions on Power Electronics-accepted*.

Egretzberger, M. and Kugi, A. (2010). A dynamical envelope model for vibratory gyroscopes. *Microsyst. Technol.*, 16, pp. 777–786.

IEEE Power Engineering Society (2004). *IEEE Guide for Field Testing of Shielded Power Cable Systems Using Very Low Frequency (VLF)*. IEEE Std. 400.2.

Krüger, M., Feurstein, R., and Filz, A. (1990). New very low frequency methods for testing extruded cables. In *Proc. of the 1990 Int. Symposium on Electrical Insulation*, 286–289. Toronto, Canada.

Mohaupt, P. and Bergmann, A. (2010). A new concept for test equipment for testing large hv and uhv cables on-site. *e&i Elektrotechnik und Informationstechnik*, 127(12), pp. 350–353.

Mohaupt, P., Geyer, H., Bergman, B., Bergman, S., Bergman, A., Kemmetmüller, W., Eberharter, S., and Kugi, A. (2012). Extension and optimization of the load range of drt test systems for testing extra-long hv and uhv cables. *e&i Elektrotechnik und Informationstechnik*, 129/7-8, 483–487.

Muhr, M., Sumereder, C., and Woschitz, R. (2001). The use of the 0,1 hz cable testing method as substitution to 50 hz measurement and the application for pd measuring and cable fault location. In *Proc. of the 12th Int. Symposium on High Voltage Engineering*. Bangalore, India.

Papoulis, A. (1962). *The Fourier Integral and its Applications*. McGraw-Hill, 1 edition.

Pietsch, R. and Hausschild, W. (2005). Hv on-site testing with partial discharge measurement. In *Brochure of the CIGRE Working Group D1.33.05*.

Putter, H., Götz, D., Petzold, F., and Oetjen, H. (2012). The evolution of vlf testing technologies over the past two decades. In *Proc. of the Transmission and Distribution Conference and Exposition*, 1–4. Orlando, Florida.

Sanders, J.A. and Verhulst, F. (1985). *Averaging Methods in Nonlinear Dynamical Systems*. Springer, New York.